Volterra Series Based Time-domain Macro-modeling of Nonlinear Circuits

Xiaoyan Y. Z. Xiong, *Member, IEEE,* Li Jun Jiang, *Senior Member, IEEE,* José E. Schutt-Ainé, *Fellow, IEEE,* and Weng Cho Chew *Fellow, IEEE,*

Abstract—**Volterra series representation is a powerful mathematical model for nonlinear circuits. However, the difficulties in determining higher-order Volterra kernels limited its broader applications. In this work, a systematic approach that enables a convenient extraction of Volterra kernels from X-parameters is presented. A concise and general representation of the output response due to arbitrary number of input tones is given. The relationship between Volterra kernels and X-parameters is explicitly formulated. An efficient frequency sweep scheme and an output frequency indexing scheme are provide. The least square linear regression method is employed to separate different orders of Volterra kernels at the same frequency, which leads to the obtained Volterra kernels complete. The proposed Volterra series representation based on X-parameters is further validated for time domain verification. The proposed method is systematic and general-purpose. It paves the way for time domain simulation with X-parameters and constitutes a powerful supplement to existing blackbox macro-modeling methods for nonlinear circuits.**

Index Terms—**Volterra series, X-parameters, nonlinear circuits, blackbox macro-modeling.**

I. INTRODUCTION

THE macro-modeling of nonlinear devices and systems is a topic of growing interest due to the dramatic increases in the complexity and size of modern systems [1]–[6]. The basic idea of macro-modeling of a circuit system is to replace the original system by an approximating system which requires much less design time and fewer resources. Building macro-models is key for enabling complete system verification and high-level design exploration. Recently developed nonlinear macro-modeling methods can be largely categorized into two major classes: nonlinear model order reduction (MOR) and nonlinear blackbox macro-model generation. Both approaches are substantially harder than their linear counterparts. The first type works directly on the SPICE level schematics, i.e., state equation derived from modified nodal analysis (MNA) method. For nonlinear MOR, a traditional method is to first linearize the system then extend projection-based MOR techniques for linear systems to accommodate nonlinear systems [7]–[10]. By doing this, the nonlinear MOR task is re-cast as the reduction of a series of linear systems. However, this method suffers

X. Y.Z. Xiong and L. J. Jiang are with the Department of Electrical and Electronic Engineering, University of Hong Kong, Pokfulam Road, Hong Kong, China (e-mail: xyxiong@eee.hku.hk; jianglj@hku.hk).

J. Schutt-Ainé and W. C. Chew are with the Department of Electrical and Computer Engineering, University of Illinois at Urbana-Champaign, Urbana, IL 61801 USA (e-mail: jschutt@emlab.uiuc.edu; w-chew@uiuc.edu). W. C. Chew was with the Faculty of Engineering, University of Hong Kong, Hong Kong.

from the exponentially increased dimension. Its relevant system transfer function is prohibitively too difficult to expand and to generate moments, essentially limiting the approach to weakly nonlinear systems. The trajectory-based piecewise-linear (TPWL) approximation approach models a nonlinear system using a collection of weighted linear models based upon a state trajectory generated by a training input [11]. Then each linear model is reduced using linear MOR techniques. This approach has the potential capability to handle large nonlinearities, but is limited by the training input dependency.

The above-mentioned nonlinear MOR methods are based on SPICE level modeling. However, in some situations, it is difficult to obtain the SPICE model due to intellectual property restrictions and limited information. Some systems cannot be described by SPICE level models because of coupling effects, distributed elements, and higher-order modes (excited by via, connector), etc. [12]. Consequently, blackbox macro-modeling becomes a viable alternative. The goal of blackbox macro-modeling is to find a mathematical relation that can reproduce the electrical behavior at the ports without any assumption about the device's internal structure. However, it is difficult to find accurate and efficient models to characterize the nonlinear behavior of devices under arbitrary loads and input signals. S-parameters are the network parameters that have been used widely as a blackbox macromodel in the signal integrity and RF/microwave frequency domains [13]–[16]. But the applicability of S-Parameters has been limited to small signals and linear behaviors.

The recently developed X-parameters from the poly-harmonic distortion (PHD) model [17] are a superset of S-parameters. They describe the relationships between incident and scattered waves by using not only port-to-port but also harmonic-to-harmonic interactions under certain large signal operating points (LSOPs). They have been successfully used to describe various nonlinear devices [18]. In the descriptive function concept, input signals are restricted to fundamental components consisting of LSOPs superposed with small harmonics. Consequently, X-parameters, essentially a frequency-domain tool, cannot support time domain simulations and have difficulty handling input signals with high peak-to-average ratios that will excite the device over broad linear and nonlinear operating ranges.

Dynamic X-parameters [19]–[21] is a fundamental extension of X-parameters to modulation-induced baseband memory effects. It can be used to model hard nonlinear behavior and long term memory effects and is valid for all possible modulation formats, for all possible peak-to-average ratios and

for a wide range of modulation bandwidths. The model can be implemented in a commercial complex envelope simulator. The core of dynamic X-parameters is the memory kernel function derived from hidden variables concept. The memory kernel can be regarded as the nonlinear impulse response of the system and can be uniquely identified from the set of complex envelope time domain measurement from initial states to final states. However, the current dynamic X-parameters model is defined in the envelope domain under several basic assumptions. The incident waves and scattered waves are restricted to be complex envelope representations of modulated carriers.

The Volterra series representation is another popular black-box macro-modeling approach for describing nonlinear devices with memory [22]–[24]. It can support time domain simulation with arbitrary input and is valid for signals that can excite both linear and nonlinear responses. Without knowing the state equation, the difficulty in determining higher-order Volterra kernels has restricted its application. We previously proposed a method to get Volterra kernels from X-parameters [25]. However, in [25], the Volterra kernel model is used as a frequency domain model. The input is restricted to harmonic input. It provides no more information than X-parameters and is unable to conduct time domain simulation. In this paper, we have extended the Volterra kernel model to time domain simulation. To make the paper more easily readable and self-contained, some formulas are rewritten and additional formulas are provided with detailed explanation. The accuracy and capability of Volterra kernel model for time domain simulation have been verified. A concise and general representation of the output responses due to arbitrary number of input tones is given. The generalized relationship between Volterra kernels and X-parameters is explicitly formulated. In addition, the requirements of the input signal are discussed in detail. An efficient frequency sweep scheme and an output frequency indexing scheme are provide. With these schemes and the symmetry property of Volterra kernels, there is no need to determine the irreducible frequency sweeping region, which makes the kernel determination procedure more convenient for computer programming. The Volterra kernels are extracted only once, which can be repeatedly used for different types of input. The proposed method is systematic and general-purpose. It is very useful for the blackbox macro-modeling of nonlinear circuits.

The organization of the paper is as follows. Section II provides a brief description of Volterra series theory. Section III gives the X-parameters formalism with incommensurate multi-tone input. Section IV presents the detailed technical description of the Volterra kernel extraction process. In Section V, numerical examples of extracting Volterra series from the X-parameters are provided. Time domain outputs are presented to validate the proposed method. Finally, a conclusion is given in Section VI.

II. VOLTERRA SERIES

Volterra series have been widely used to characterize nonlinear systems with memory [26]. For a system with input $u(t)$, the output $y(t)$ can be expressed using the expansion

$$y(t) = \sum_{n=1}^{\infty} y_n(t) \tag{1}$$

with

$$y_n(t) = \frac{1}{n!} \int_{-\infty}^{+\infty} \cdots \int_{-\infty}^{+\infty} h_n(\tau_1, \ldots, \tau_n) \cdot \tag{2}$$
$$u(t - \tau_1) \ldots u(t - \tau_n) d\tau_1 \ldots d\tau_n$$

where $h_n(\tau_1, \ldots, \tau_n)$ is the nth-order time domain Volterra kernel or impulse response. In particular, $y_1(t)$ is the usual first-order convolution having its frequency domain representation

$$Y_1(\omega) = H_1(\omega)U(\omega) \tag{3}$$

where $H_1(\omega) = \int_{-\infty}^{+\infty} h_1(\tau)e^{-j\omega\tau}d\tau$ is the linear transfer function or the first-order Volterra kernel. $U(\omega)$ is the Fourier transform of $u(t)$. However, the nonlinear higher-order output cannot be written in a form similar to (3). By replacing the single time axis by multiple time axes, (2) becomes

$$y_n(t_1, \ldots, t_n) = \frac{1}{n!} \int_{-\infty}^{+\infty} \cdots \int_{-\infty}^{+\infty} h_n(\tau_1, \ldots, \tau_n) \cdot \tag{4}$$
$$u(t_1 - \tau_1) \ldots u(t_n - \tau_n) d\tau_1 \ldots d\tau_n$$

The frequency domain representation of (4) can be conveniently written in a form similar to (3)

$$Y_n(\omega_1, \ldots, \omega_n) = H_n(\omega_1, \ldots, \omega_n)U(\omega_1) \ldots U(\omega_n) \tag{5}$$

with the nonlinear transfer function H_n defined as

$$H_n(\omega_1, \ldots, \omega_n) = \int_{-\infty}^{+\infty} \cdots \int_{-\infty}^{+\infty} h_n(\tau_1, \ldots, \tau_n) \cdot \tag{6}$$
$$e^{-j\omega_1\tau_1} \ldots e^{-j\omega_n\tau_n} d\tau_1 \ldots d\tau_n$$

To restore $y_n(t)$, one then evaluates along the diagonal line in the multi-time hyperplane

$$y_n(t) = y_n(t_1, \ldots, t_n)|_{t_1=t_2=\ldots=t_n=t} \tag{7}$$

where $y_n(t_1, \ldots, t_n)$ is the multidimensional inverse Fourier transform of $Y_n(\omega_1, \ldots, \omega_n)$.

III. X-PARAMETERS FORMALISM

X-parameters, derived from the polyharmonic distortion (PHD) model [17], [27], are a superset of S-parameters and can be used to describe the behavior of nonlinear devices in the frequency domain. For better clarification and without losing generality, we take the incommensurate 3-tone excitation case to illustrate the formalism of X-parameters [28]. Suppose the incident signal $A_q(t)$ at port q has three large incommensurate fundamental tones with frequencies ω_1, ω_2 and ω_3. They are incommensurate if the ratio of their frequencies is irrational:

$$k_1\omega_1 + k_2\omega_2 + k_3\omega_3 = 0 \Rightarrow k_1 = k_2 = k_3 = 0 \tag{8}$$
$$\text{for } k_1, k_2, k_3 \in \mathbb{Z}$$

The scattered signal at port p contains numerous frequency components. They are the combinations of the input tones $\omega = k_1\omega_1 + k_2\omega_2 + k_3\omega_3$ and can be indexed as $B_{p,[k_1,k_2,k_3]}$.

Then, X-parameters are used to link the scattered signal B with incident signal A under linearization around specific LSOPs (amplitudes and phases of input tones, bias, loads, etc.).

$$
\begin{aligned}
B_{p,[k_1,k_2,k_3]} = & \; X^{(F)}_{p,[k_1,k_2,k_3]} P^{k_1}_{[1,0,0]} P^{k_2}_{[0,1,0]} P^{k_3}_{[0,0,1]} \quad (9) \\
& + \sum_{q,k_1',k_2',k_3'} \Big[X^{(S)}_{p,[k_1,k_2,k_3];q,[k_1',k_2',k_3']} P^{k_1-k_1'}_{[1,0,0]} P^{k_2-k_2'}_{[0,1,0]} P^{k_3-k_3'}_{[0,0,1]} \\
& \qquad\qquad A_{q,[k_1',k_2',k_3']} \Big] \\
& + \sum_{q,k_1',k_2',k_3'} \Big[X^{(T)}_{p,[k_1,k_2,k_3];q,[k_1',k_2',k_3']} P^{k_1+k_1'}_{[1,0,0]} P^{k_2+k_2'}_{[0,1,0]} P^{k_3+k_3'}_{[0,0,1]} \\
& \qquad\qquad A^*_{q,[k_1',k_2',k_3']} \Big]
\end{aligned}
$$

The $X^{(F)}$ term includes the information of the three large fundamental tones $A_{q,[1,0,0]}, A_{q,[0,1,0]}$ and $A_{q,[0,0,1]}$. $P_{[1,0,0]}$, $P_{[0,1,0]}$ and $P_{[0,0,1]}$ are the initial phases of input tones. $X^{(S)}$ and $X^{(T)}$ are scattering parameters describing the small signal interactions under spectral linearization around the LSOPs. $X^{(S)}_{p,[k_1,k_2,k_3];q,[k_1',k_2',k_3']}$ is a scattering parameter of type S that accounts for the contribution to the frequency indexed as $[k_1, k_2, k_3]$ of the scattered wave at port p from the $[k_1', k_2', k_3']$-th harmonic of the incident wave at port q. $X^{(T)}$ is a scattering parameter of type T. The definitions of the subscripts of $X^{(T)}$ are the same as those of the $X^{(S)}$ term except that they account for the contribution from harmonics of the conjugate of the incident wave. The existence of a scattering parameter of type T is due to the nonanalyticity of the spectral mapping from the time domain to the frequency domain [27]. The sum runs over all q and all integers k_1', k_2', k_3'.

IV. VOLTERRA KERNEL EXTRACTION FROM X-PARAMETERS

A. Determination of Volterra Kernels

Volterra kernels are transfer functions of a nonlinear system and are widely used to characterize a nonlinear system with memory. Previously, Volterra kernels are calculated by the harmonic input method [26], [29], [30]. However, the determination process is very tedious and time-consuming. It requires the generation of input tones, waiting for steady-state, sampling the output, computation of Fourier transfer to get the output response at distinct frequencies. When frequency sweep is needed, the determination task becomes extremely challenging especially for high-order kernels. On the other hand, X-parameters can be conveniently obtained from harmonic-balance (HB) simulation or measured by modern nonlinear vector network analyzers (NVNA). Inspired by the formalism of the incommensurate multi-tone X-parameters, we propose a systematic method to obtain the Volterra series representation of X-parameters based on the concept of harmonic input method. In this work, we take the negative frequencies into account by adding the complex conjugation terms and give the general representation of the output responses due to harmonic inputs. In general, to get the complete description of the Mth-order Volterra kernel, an M-tone excitation is required. Suppose the input signal is the superposition of M

incommensurate tones

$$
u(t) = \sum_{m=1}^{M} \frac{V_m}{2} e^{j\omega_m t} + \text{c.c.} = \sum_{\substack{m=-M \\ m\neq 0}}^{M} \frac{V_m}{2} e^{j\omega_m t} \quad (10)
$$

where "c.c." denotes the complex conjugate terms, and $\omega_{-m} = -\omega_m$, and $V_{-m} = V_m^*$, m is an integer. Substituting the input representation (10) into (2), the nth-order output is

$$
\begin{aligned}
y_n(t) = & \frac{1}{n!} \int_{-\infty}^{+\infty} \cdots \int_{-\infty}^{+\infty} h_n(\tau_1, \ldots, \tau_n) \cdot \quad (11) \\
& \prod_{i=1}^{n} \left[\frac{V_1}{2} e^{j\omega_1(t-\tau_i)} + \cdots + \frac{V_M}{2} e^{j\omega_M(t-\tau_i)} + \text{c.c.} \right] d\bar{\tau} \\
= & \frac{1}{n!} \sum_{m_1=-M}^{M} \cdots \sum_{m_n=-M}^{M} \left[\prod_{i=1}^{n} \frac{V_{m_i}}{2} \right] \cdot \\
& H_n^{sym}(\omega_{m_1}, \ldots, \omega_{m_n}) \cdot \exp\left(j \sum_{i=1}^{n} \omega_{m_i} t \right)
\end{aligned}
$$

where m_i is an integer and $m_i \neq 0$, $d\bar{\tau} = d\tau_1 \ldots d\tau_n$. $H_n^{sym}(\cdot)$ in (11) is defined as the nth symmetric frequency domain Volterra kernel or transfer function. The symmetric kernel satisfies

$$
H_n^{sym}(\omega_1, \omega_2, \ldots, \omega_n) = H_n^{sym}(\omega_{m_1}, \omega_{m_2}, \ldots, \omega_{m_n}) \quad (12)
$$

where the subscript of the argument m_i denotes any permutation of the integers $1, \ldots, n$. It can be obtained by setting [30]

$$
H_n^{sym}(\cdot) = \frac{1}{n!} \sum_{\substack{\text{all permutations of} \\ \{\omega_{m_1}, \ldots, \omega_{m_n}\}}} H_n^{asym}(\omega_{m_1}, \ldots, \omega_{m_n}) \quad (13)
$$

In this paper, we use symmetric Volterra kernel. The superscript "sym" is omitted for simplicity. Some of the values $\omega_{m_1}, \ldots, \omega_{m_n}$ may be repeated. Thus, many terms in (11) contain identical exponents. Taking a three-tone excitation ($M = 3$) as an example, the third-order output $y_3(t)$ in (11) contains 216 third-order Volterra kernels. The arguments ω_{m_i} of these kernels $H_3(\omega_{m_1}, \omega_{m_2}, \omega_{m_3})$ can be $\pm\omega_1$, $\pm\omega_2$ and $\pm\omega_3$. The Volterra kernels included in $y_3(t)$ are $H_3(-\omega_1,\omega_1,\omega_1)$, $H_3(\omega_1,-\omega_1,\omega_1)$, $H_3(\omega_1,\omega_1,-\omega_1)$, $H_3(\omega_1,\omega_2,-\omega_2)$, $H_3(\omega_1,-\omega_2,\omega_2)$, $H_3(\omega_2,\omega_1,-\omega_2)$, $H_3(-\omega_2,\omega_1,\omega_2)$, $H_3(\omega_2,-\omega_2,\omega_1)$, $H_3(-\omega_2,\omega_2,\omega_1)$, etc. Due to the permutation symmetry, the first three kernels are the same and corresponding to the output frequency $\omega = \omega_{m_1} + \omega_{m_2} + \omega_{m_3} = 2\omega_1 - \omega_1 = \omega_1$. The next six kernels are the same and also corresponding to the output frequency $\omega = \omega_1 + \omega_2 - \omega_2 = \omega_1$. These symmetric Volterra kernels coinciding at the same frequency can be collected together. We introduce a concise kernel $G_{[k_1+r_1,r_1],\ldots,[k_M+r_M,r_M]}(\omega_1, \ldots, \omega_M)$ to denote all symmetric kernels at frequency $k_1\omega_1 + k_2\omega_2 + \cdots + k_M\omega_M$ (k_m is an integer and $0 \leq |k_m| \leq n$).

$G_{[k_1+r_1,r_1],\ldots,[k_M+r_M,r_M]}(\omega_1, \ldots, \omega_M)$ is $H_n(\omega_{m_1}, \ldots,$

ω_{m_n}) with

$$
\begin{aligned}
k_1 + 2r_1 + \ldots + k_M + 2r_M &= n \qquad (14) \\
\text{first } k_1 + r_1 \text{ of } \omega_{m_i} &= +\omega_1 \\
\text{next } r_1 \text{ of } \omega_{m_i} &= -\omega_1 \\
&\vdots \\
\text{next } k_M + r_M \text{ of } \omega_{m_i} &= +\omega_M \\
\text{next } r_M \text{ of } \omega_{m_i} &= -\omega_M
\end{aligned}
$$

The number of arguments of $G(\cdot)$ is equal to the number of excitation tones. The number of arguments of $H(\cdot)$ is $k_1 + 2r_1 + \ldots + k_M + 2r_M$. The mth subscript of $G(\cdot)$ kernel $[k_m + r_m, r_m]$ corresponds to the arguments ω_m of $H(\cdot)$ (with $k_m + r_m$ positive ω_m and r_m negative ω_m arguments). Hence, in the three-tone excitation example, the first three kernels, e.g., $H_3(\omega_1, \omega_1, -\omega_1)$, can be rewritten as $G_{[1+1,1],[0+0,0],[0+0,0]}(\omega_1, \omega_2, \omega_3)$ (with $k_1 = r_1 = 1$, $k_2 = r_2 = k_3 = r_3 = 0$ in the general representation of $G(\cdot)$). That is, the first $k_1 + r_1 = 2$ arguments of H_3 are ω_1; the next $r_1 = 1$ argument is $-\omega_1$. Similarly, the next six kernels, e.g., $H_3(\omega_1, \omega_2, -\omega_2)$, can be denoted as $G_{[1+0,0],[0+1,1],[0+0,0]}(\omega_1, \omega_2, \omega_3)$ (with $k_1 = r_2 = 1$, $r_1 = k_2 = k_3 = r_3 = 0$ in the general representation of $G(\cdot)$). That is, the first $k_1 + r_1 = 1$ argument is ω_1; the next $r_1 = 0$ argument is $-\omega_1$; the next $k_2 + r_2 = 1$ argument is ω_2; and the next $r_2 = 1$ argument is $-\omega_2$. By using the new kernel representation and collecting all terms at frequency $k_1\omega_1 + k_2\omega_2 + \cdots + k_M\omega_M$, we get a simplified representation of (11)

$$
\begin{aligned}
y_n(t) = \sum_{r_1} \cdots \sum_{r_M} &\left[\left(\frac{V_1}{2}\right)^{k_1+r_1} \left(\frac{V_1^*}{2}\right)^{r_1} \cdots \left(\frac{V_M}{2}\right)^{k_M+r_M} \right. \\
&\left. \left(\frac{V_M^*}{2}\right)^{r_M} \right] \cdot \left[(k_1+r_1)! r_1! \ldots (k_M+r_M)! r_M! \right]^{-1} \\
&\cdot G_{[k_1+r_1,r_1],\ldots,[k_M+r_M,r_M]}(\omega_1,\ldots,\omega_M) \\
&\cdot \exp\left[j(k_1\omega_1 + \ldots + k_M\omega_M)t\right] \qquad (15)
\end{aligned}
$$

where r_m are nonnegative integer indices that satisfy $k_1 + 2r_1 + k_2 + 2r_2 + \ldots + k_M + 2r_M = n$ since $G_{[k_1+r_1,r_1],\ldots,[k_M+r_M,r_M]}(\cdot)$ is the nth-order kernel. The number of symmetric kernels denoted by $G_{[k_1+r_1,r_1],\ldots,[k_M+r_M,r_M]}(\cdot)$ is $\frac{n!}{(k_1+r_1)! r_1! \ldots (k_M+r_M)! r_M!}$. When $k_m < 0$, the signs of ω_m are reversed, e.g., if $k_1 < 0$, the first $|k_1| + r_1$ arguments of H_n are $-\omega_1$ and the next r_1 arguments are $+\omega_1$. For example, $H_3(-\omega_1, \omega_2, \omega_2)$ corresponds to the output frequency $\omega = -\omega_1 + 2\omega_2$. It is denoted by $G_{[-1+0,0],[2+0,0],[0+0,0]}$ with $k_1 = -1 < 0$. Then we reverse the sign of ω_1. Now the first $|k_1| + r_1 = 1$ argument becomes $-\omega_1$.

The general representation of the total output $y(t)$ due to an M-tone excitation is similar to (15) except that all r_m go from zero to infinity.

$$
\begin{aligned}
y(t) = \sum_{r_1=0}^{\infty} \cdots \sum_{r_M=0}^{\infty} &\left[\left(\frac{V_1}{2}\right)^{k_1+r_1} \left(\frac{V_1^*}{2}\right)^{r_1} \cdots \left(\frac{V_M}{2}\right)^{k_M+r_M} \right. \\
&\left. \left(\frac{V_M^*}{2}\right)^{r_M} \right] \cdot \left[(k_1+r_1)! r_1! \ldots (k_M+r_M)! r_M! \right]^{-1} \\
&\cdot G_{[k_1+r_1,r_1],\ldots,[k_M+r_M,r_M]}(\omega_1,\ldots,\omega_M) \\
&\cdot \exp\left[j(k_1\omega_1 + \ldots + k_M\omega_M)t\right] \qquad (16)
\end{aligned}
$$

The Volterra kernels can be determined once the magnitudes and phases of the corresponding frequency components of the output signal $Y(k_1\omega_1 + \ldots + k_M\omega_M)$ are known. The information is provided by X-parameters. Once we know the mapping relationship between the output response due to an m-tone excitation and the m-tone X-parameters, we can calculate the mth-order Volterra kernels.

B. Relationship between Volterra Kernels and X-parameters

As discussed above, the determination of the M-th Volterra kernel requires an M-tone input signal. With multi-tone input, mixing products will occur. The maximum mixing order M_0 is defined as the maximum order of the intermodulation terms included in the output frequency list. For example, assume there are two fundamental tones ω_1 and ω_2. If $M_0 = 0$ or 1, no mixing products are included in the output frequency list; if $M_0 = 2$, the $\pm|\omega_1 \pm \omega_2|$ intermodulation terms are included; if $M_0 = 3$, additional $\pm|2\omega_1 \pm \omega_2|$ and $\pm|\omega_1 \pm 2\omega_2|$ terms are included. For better presentation, the $M = 3$ case is used to illustrate the relationship between Volterra kernels and X-parameters. The maximum order of each tone is M and the maximum mixing order M_0 is also set to $M_0 = M$. In addition, thanks to the time invariant property [27], the initial phase of each tone is set to zero ($V_m = V_m^*$). Based on (9) and (14), we can link Volterra kernels with X-parameters by equating the same frequency component of the output signal, i.e., by setting $Y(k_1\omega_1 + k_2\omega_2 + k_3\omega_3) = B_{p,[k_1,k_2,k_3]}$. Table I gives the mapping between Volterra kernels and X-parameters of the first four frequency components.

As shown in Table I, each frequency component contains the contribution from numerous Volterra kernels. Take the output frequency with index $[k_1, k_2, k_3] = [0, 0, 1]$ as an example. The output frequency is $\omega = k_1\omega_1 + k_2\omega_2 + k_3\omega_3 = \omega_3$. According to (16), the phasor of this frequency component can be written as:

$$
\begin{aligned}
Y(\omega_3) =& \sum_{r_1=0}^{\infty} \sum_{r_2=0}^{\infty} \sum_{r_3=0}^{\infty} \left[\frac{(V_1/2)^{2r_1}(V_2/2)^{2r_2}(V_3/2)^{1+2r_3}}{(r_1!)^2(r_2!)^2(1+r_3)! r_3!} \right] \\
&\cdot G_{[0+r_1,r_1],[0+r_2,r_2],[1+r_3,r_3]}(\omega_1, \omega_2, \omega_3) \\
=& \; B_{p,[0,0,1]} \qquad (17)
\end{aligned}
$$

when r_1, r_2 and r_3 run from zero to infinity, we can list the Volterra kernels included in (17) according to (14)

TABLE I
THE MAPPING BETWEEN VOLTERRA KERNELS AND X-PARAMETERS OF A TWO PORTS NETWORK

Frequency index $[k_1, k_2, k_3]$	Phasor $Y(k_1\omega_1 + k_2\omega_2 + k_3\omega_3)$	Volterra Kernels	X-parameters
$[0, 0, 1]$	$Y(\omega_3)$	$\frac{V_3}{2}H_1(\omega_3) + \frac{V_3^3}{16}H_3(\omega_3, \omega_3, -\omega_3) + \frac{V_3 V_2^2}{8}H_3(\omega_3, \omega_2, -\omega_2) +$ $\frac{V_3 V_1^2}{8}H_3(\omega_3, \omega_1, -\omega_1) + \frac{V_3^5}{384}H_5(\omega_3, \omega_3, \omega_3, -\omega_3, -\omega_3) + \ldots$	$B_{2,[0,0,1]}$
$[0, 0, 2]$	$Y(2\omega_3)$	$\frac{V_3^2}{8}H_2(\omega_3, \omega_3) + \frac{V_3^4}{96}H_4(\omega_3, \omega_3, \omega_3, -\omega_3) +$ $\frac{V_3^2 V_2^2}{32}H_4(\omega_3, \omega_3, \omega_2, -\omega_2) + \ldots$	$B_{2,[0,0,2]}$
$[0, 0, 3]$	$Y(3\omega_3)$	$\frac{V_3^3}{48}H_3(\omega_3, \omega_3, \omega_3) + \frac{V_3^5}{768}H_5(\omega_3, \omega_3, \omega_3, \omega_3, -\omega_3) +$ $\frac{V_3^3 V_2^2}{192}H_5(\omega_3, \omega_3, \omega_3, \omega_2, -\omega_2) + \ldots$	$B_{2,[0,0,3]}$
$[0, 1, -2]$	$Y(\omega_2 - 2\omega_3)$	$\frac{V_2 V_3^2}{16}H_3(\omega_2, -\omega_3, -\omega_3) + \frac{V_2 V_3^4}{192}H_5(\omega_2, -\omega_3, -\omega_3, -\omega_3, \omega_3) +$ $\cdots$	$B_{2,[0,1,-2]}$

$$
\begin{aligned}
r_1 = r_2 = r_3 = 0 : \quad & H_1(\omega_3) \quad (18)\\
r_1 = r_2 = 0 \text{ and } r_3 = 1 : \quad & H_3(\omega_3, \omega_3, -\omega_3)\\
r_1 = r_3 = 0 \text{ and } r_2 = 1 : \quad & H_3(\omega_2, -\omega_2, \omega_3)\\
r_2 = r_3 = 0 \text{ and } r_1 = 1 : \quad & H_3(\omega_1, -\omega_1, \omega_3)\\
r_1 = r_2 = 0 \text{ and } r_3 = 2 : \quad & H_5(\omega_3, \omega_3, \omega_3, -\omega_3, -\omega_3)\\
& \vdots \qquad\qquad \vdots
\end{aligned}
$$

Consequently, (17) can be expanded and rewritten as

$$
\begin{aligned}
Y(\omega_3) =\ & \frac{V_3}{2}H_1(\omega_3) + \frac{V_3^3}{16}H_3(\omega_3, \omega_3, -\omega_3) + \quad (19)\\
& \frac{V_3 V_2^2}{8}H_3(\omega_2, -\omega_2, \omega_3) +\\
& \frac{V_3 V_1^2}{8}H_3(\omega_1, -\omega_1, \omega_3) +\\
& \frac{V_3^5}{384}H_5(\omega_3, \omega_3, \omega_3, -\omega_3, -\omega_3) + \ldots\\
=\ & B_{p,[0,0,1]}
\end{aligned}
$$

As presented in (19), the output at frequency ω_3 contains different orders of Volterra kernels: the linear term $H_1(\omega_3)$, the compression term $H_3(\omega_3, \omega_3, -\omega_3) \triangleq H_{3c}$, the desensitization terms $H_3(\omega_2, -\omega_2, \omega_3) \triangleq H_{3d2}, H_3(\omega_1, -\omega_1, \omega_3) \triangleq H_{3d1}$ and other higher-order terms with $n > 3$. We need to separate these kernels.

C. Separation of Volterra Kernels

In general, the magnitude of high-order output decreases drastically as the magnitude of the input signal decreases even though the magnitude of higher-order kernel may be large. For instance, supposing the input signal is denoted as $\alpha u(t)$ (with $\alpha u(t) < 1$), then the nth-order output $y_n(t)$ is proportional to $\alpha^n u^n(t)$ according to (2). Thus, if the input is reduced by 3 dB, $y_1(t)$ falls by 3 dB, $y_2(t)$ falls by 6 dB and so on. The separation of Volterra kernels makes use of this property. Provided that the magnitude of the input signal $u(t)$ is smaller than some upper bound, the high order terms above M are negligible. By setting an input signal with

suitable magnitude, the infinite summation for each frequency component is truncated to a finite one by ignoring the higher-order terms. Then the kernels can be separated based on the least square linear regression method [31] in the frequency domain. The basic idea consists of arranging the magnitudes of the input tones so that a matrix can be constructed for the kernels. Take (19) as an example and ignore the higher-orders with $n > 3$ by changing V_3, a matrix equation is constructed:

$$
\begin{bmatrix}
\frac{V_3^{(1)}}{2} & \frac{\left(V_3^{(1)}\right)^3}{16} & \frac{V_3^{(1)} V_2^2}{8} & \frac{V_3^{(1)} V_1^2}{8}\\
\frac{V_3^{(2)}}{2} & \frac{\left(V_3^{(2)}\right)^3}{16} & \frac{V_3^{(2)} V_2^2}{8} & \frac{V_3^{(2)} V_1^2}{8}\\
\frac{V_3^{(3)}}{2} & \frac{\left(V_3^{(3)}\right)^3}{16} & \frac{V_3^{(3)} V_2^2}{8} & \frac{V_3^{(3)} V_1^2}{8}\\
\frac{V_3^{(4)}}{2} & \frac{\left(V_3^{(4)}\right)^3}{16} & \frac{V_3^{(4)} V_2^2}{8} & \frac{V_3^{(4)} V_1^2}{8}
\end{bmatrix}
\begin{bmatrix}
H_1\\
H_{3c}\\
H_{3d2}\\
H_{3d1}
\end{bmatrix} \quad (20)
$$
$$
= \begin{bmatrix} Y(\omega_3)^{(1)} & Y(\omega_3)^{(2)} & Y(\omega_3)^{(3)} & Y(\omega_3)^{(4)} \end{bmatrix}^T
$$

where $V_3^{(i)}$, $i = 1, \ldots, 4$, are some properly chosen magnitudes of the third tone and $Y(\omega_3)^{(i)}$ are the corresponding phasors of the frequency component ω_3. Different Volterra kernels are the solutions of (20). It is essential that the magnitudes of the input tones are properly chosen. They should be smaller than some upper bound so that lower-order Volterra kernels will not be skewed by high order terms but not so small that the higher-order terms will be buried in the noise. One improvement is to add additional input magnitudes and use the least square solutions of the resulting overdetermined equation as the estimate of the kernels. The magnitudes of the other two tones V_1 and V_2 are also changed to form the overdetermined matrix equation. However, with the increasing number of higher order Volterra kernels being included, the kernel separation becomes much harder even with the least square method. The least square method may give poor estimates of the kernels. One remedy is that we can first get good estimates of low order kernels by properly choosing small magnitudes of input tones; then conduct an additional least square estimate for the higher order kernels by setting low order kernels as knowns to reduce the error propagation.

D. Design of Input Signal

To obtain a complete description of Volterra kenels $H_1(\omega_1)$, $H_2(\omega_1, \omega_2)$ and $H_3(\omega_1, \omega_2, \omega_3)$, frequency sweep along axes ω_1, ω_2 and ω_3 in the interested region is required. In addition, for convenient kernel separation, output frequencies are required to be distinct from each other. Hence, careful attention must be paid in choosing the frequency components included in the input signal. With incommensurate input tones, this condition is satisfied automatically. However, it is difficult to ensure the incommensurate condition for all combinations of sweeping frequencies. In practice, the incommensurate requirement can be relaxed as follows: suppose the number of frequency sweeping points along the ω_α axis is N_α with $\alpha = 1, 2, 3$ ($M = 3$ case); by carefully choosing the input frequencies $\omega_{1,i}$, $\omega_{2,j}$, and $\omega_{3,k}$, the output frequencies will not overlap with each other. Here, i, j and k are integers with $1 \le i \le N_1$, $1 \le j \le N_2$, and $1 \le k \le N_3$. Hence, we need to choose the input frequencies such that

$$k_1\omega_{1,i} + k_2\omega_{2,j} + k_3\omega_{3,k} = k_1'\omega_{1,i} + k_2'\omega_{2,j} + k_3'\omega_{3,k} \quad (21)$$
$$\text{iff } k_1 = k_1', \; k_2 = k_2' \text{ and } k_3 = k_3'$$

Equation (21) must be satisfied for all k_1, k_2, k_3, k_1', k_2', $k_3' \in \{0, \pm1, \pm2, \dots, \pm M_0\}$.

E. Notation of Output Frequency

For systems with real input and output signals in the time domain, the spectra in the frequency domain are double sided with conjugate symmetry, e.g., $H_3(\omega_1, \omega_2, -\omega_3) = H_3^*(-\omega_1, -\omega_2, \omega_3)$. Hence, the spectra contain redundant information by a factor of two. The output frequency is determined by indices k_1, k_2, and k_3, and by values of input frequencies. For some set of $[k_1, k_2, k_3]$, the output frequency can be negative. The information about these negative frequencies can be obtained from the corresponding positive frequencies with indices $[-k_1, -k_2, -k_3]$. Here, we present an indexing scheme that includes all output frequencies and meanwhile removes the redundancy. Supposing the highest-order of Volterra kernels is $M = 3$ and the maximum mixing order $M_0 = M$, then the indices of the output frequency $[k_1, k_2, k_3]$ are arranged according to the following scheme:

1) the summation of absolute values of all indices is less than or equal to the maximum mixing order (e.g., $|k_1| + |k_2| + |k_3| \le M_0$);
2) the first index is always nonnegative (e.g., $k_1 \ge 0$);
3) the first nonzero index begins with positive number (e.g., if $k_1 = k_2 = 0$, $k_3 > 0$);
4) the second nonzero index begins with the available minimum integer (e.g., if $k_1 \ne 0$, k_2 begins with $-(M_0 - |k_1|)$) and so does the next nonzero index (e.g., if $k_1 \ne 0$ and $k_2 \ne 0$, k_3 begins with $-(M_0 - |k_1| - |k_2|)$);

These conditions are listed in descending order according to priority. By using the above indexing scheme, instead of recording all combinations of $[k_1, k_2, k_3]$, only 31 frequencies need to be recorded for the $M = M_0 = 3$ case (see Appendix A for more details). When the index $[k_1, k_2, k_3]$

results in a negative frequency, the complex conjugate of the corresponding phasor is considered and its contribution is attributed to the corresponding positive frequency.

In addition, Volterra kernels also have the permutation symmetry property, e.g., $H_3(\omega_1, \omega_2, \omega_3) = H_3(\omega_1, \omega_3, \omega_2) = H_3(\omega_2, \omega_1, \omega_3) = H_3(\omega_2, \omega_3, \omega_1) = H_3(\omega_3, \omega_1, \omega_2) = H_3(\omega_3, \omega_2, \omega_1)$. For each triplet $(\omega_{1,i}, \omega_{2,j}, \omega_{3,k})$, as shown in Fig. 1, it will determine 216 points in the $H_3(\omega_1, \omega_2, \omega_3)$ space. Meanwhile, 36 and 6 points will be determined in the $H_2(\omega_1, \omega_2)$ and $H_1(\omega_1)$ space, respectively. Due to the permutation and conjugate symmetry properties of kernels, only 28 points need to be recorded for the third-order kernel, and 9 and 3 points for the second-order and first-order kernels, respectively. This leads to an efficient Volterra kernel determination process.
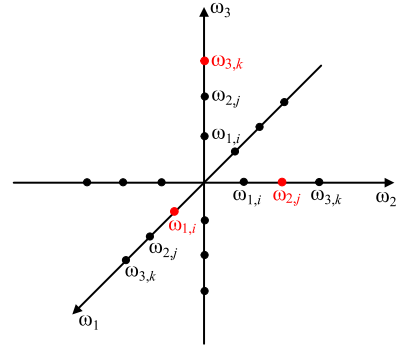

Fig. 1. Distribution of points in the $H_3(\omega_1, \omega_2, \omega_3)$ space with one triplet $(\omega_{1,i}, \omega_{2,j}, \omega_{3,k})$.

V. NUMERICAL EXAMPLES

A. A Benchmark Case

1) Description of the Nonlinear System: The first numerical example is meanwhile to benchmark a nonlinear system with known Volterra kernels. Fig. 2 shows the system diagram. H_a, H_b and H_c are frequency domain transfer functions of linear-time-invariant systems. The symbol Π denotes the time domain multiplication even though the subsystems are represented in the frequency domain. The V-I relationship at port 3 of the multiplier is

$$i_3(t) = [v_1(t)v_2(t) - v_3(t)] / Z_f \quad (22)$$

where v_j and i_j are the voltage and current at port j respectively, $j \in \{1, 2, 3\}$. $Z_f = R = 50 \, \Omega$.
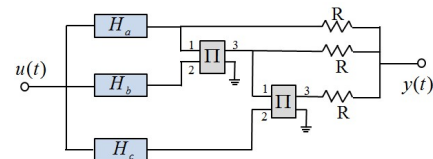

Fig. 2. System diagram of a third-order nonlinear circuit.

Because there are two multipliers, the whole system has up to the third-order nonlinearity. In the frequency domain,

Volterra kernels of the whole system have the following ideal analytical expression:

$$H_1(\omega_1) = c_1 H_a(\omega_1) \tag{23}$$
$$H_2(\omega_1, \omega_2) = c_2 \left[H_a(\omega_1) H_b(\omega_2) \right]_{\text{sym}}$$
$$H_3(\omega_1, \omega_2, \omega_3) = c_3 \left[H_a(\omega_1) H_b(\omega_2) H_c(\omega_3) \right]_{\text{sym}}$$

where $[\cdot]_{\text{sym}}$ indicates a symmetrized Volterra kernel according to (13); c_i is a constant determined by circuit parameters (e.g., Z_f, R). However, due to the mismatch between different blocks, reflections will occur and slightly modify the ideal kernel representations. We set $H_a = H_b = H_c$ as the transfer function of a low pass filter (LPF) system. Fig. 3 shows the magnitude of the transfer function H_a which is equivalent to S-parameters S_{21}.
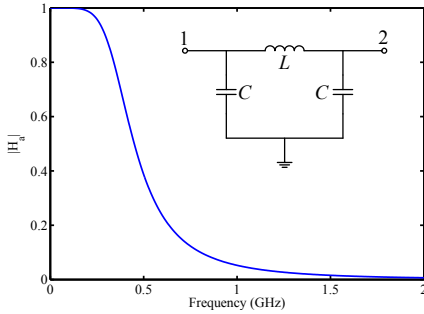
Fig. 3. Magnitude of the transfer function H_a of the low pass filter; the inset shows the circuit schematic diagram with $L = 42.52\,\text{nH}$ and $C = 8.5\,\text{pF}$.

2) Frequency Domain Volterra Kernels: Volterra kernels of the nonlinear system shown in Fig. 2 are extracted from X-parameters. The 3-tone X-parameters of the nonlinear system are generated by applying the ADS X-parameters genera-tor [32]. The frequency sweep scheme of each axis is given in Table II. Although the frequency step of each axis is 120 MHz, the equivalent frequency step is 40 MHz thanks to the symmetry properties of kernels. To separate different

TABLE II
FREQUENCY SWEEP SCHEME FOR THE 3-TONE X-PARAMETERS
GENERATION

Frequency	Start	Step	Stop
ω_1	7 MHz	120 MHz	2.047 GHz
ω_2	41 MHz	120 MHz	2.081 GHz
ω_3	87 MHz	120 MHz	2.127 GHz

order of Volterra kernels, the power of each input tone is set to $P_{in} = \{5, 10\}$ dBm. The proposed method described in Sec. IV is used to extract Volterra kernels H_1, H_2 and H_3. Fig. 4 shows the magnitude and phase of the first-order Volterra kernel. They agree well with the S-parameters of the system with small signal input. Fig. 5 and Fig. 6 present the magnitudes and phases of the second-order Volterra kernel and a slice of the third-order Volterra kernel, respectively, with ω_3 fixed at 0.5 GHz. They have reasonable distributions compared to the ideal analytical expression in (19). In addition, they also agree with the permutation and conjugate symmetric proper-ties. For example, the magnitude of H_2 has two symmetry planes: $\omega_1 = \pm\omega_2$; the phase of H_2 has a symmetry plane

$\omega_1 = \omega_2$ and an anti-symmetry plane $\omega_1 = -\omega_2$; while the third-order kernel loses the conjugate symmetry property since ω_3 is fixed. It only has one symmetry plane $\omega_1 = \omega_2$.
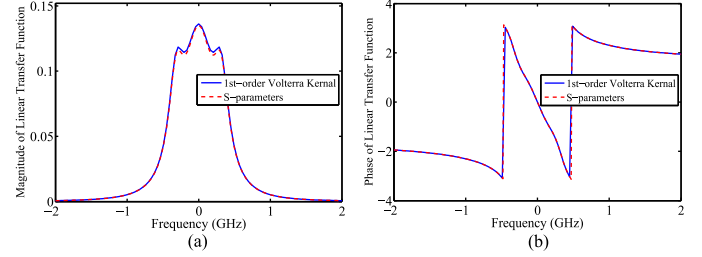
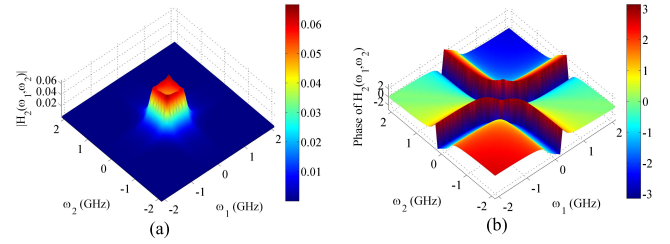Fig. 4. Magnitude and phase of the linear transfer function $H_1(\omega_1)$. (a) magnitude; (b) phase.

Fig. 5. Magnitude and phase of the second-order Volterra kernel $H_2(\omega_1, \omega_2)$; (a) magnitude; (b) phase.
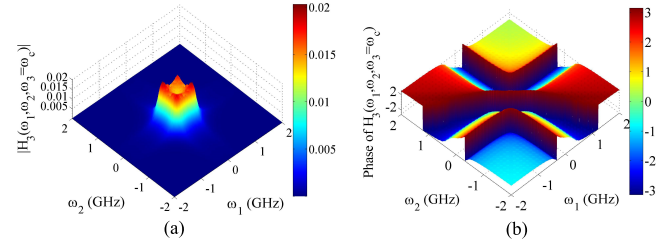
Fig. 6. Magnitude and phase of the third-order Volterra kernel $H_3(\omega_1, \omega_2, \omega_3 = \omega_c)$ with ω_c fixed to 0.5 GHz; (a) magnitude; (b) phase.

3) Time Domain Output: To validate the accuracy of the extracted Volterra kernels and to demonstrate the capability of Volterra series for time domain simulation with arbitrary input, the time domain outputs are presented. Without losing gener-ality, the input is chosen to be a rectangular pulse as shown in the inset of Fig. 7(b). The magnitude is $V_0 = 1\,\text{V}$. The input has rich frequency components as shown in Fig. 7(a). The X-parameter macro-model requires numerous fundamental tones to represent the input [33]. In addition, once the input signal changes, one needs to regenerate the X-parameter macro-model for the same system since X-parameter is defined under certain LSOPs (fixed magnitude and phase of each fundamental tone). In contrast, the same Volterra series model can be used for arbitrary input. The linear, second-order and third-order time domain responses $y_1(t)$, $y_2(t)$ and $y_3(t)$ are given in Fig. 7(b), (c) and (d), respectively. They are calculated

according to (5) and (7) with extracted Volterra kernels. The total response is the summation of both linear and nonlinear responses as indicated by (1). Fig. 8 presents the total response calculated by the Volterra series representation. It agrees very well with that obtained by ADS transient simulator with the original circuit model. However, as shown in Fig. 8, the linear response calculated by S-parameter does not agree with the response of the original circuit model. The higher-order Volterra kernels are crucial to capturing the nonlinearities of the systems. The linear response ignores the contributions of higher order Volterra kernels and hence it is incorrect.
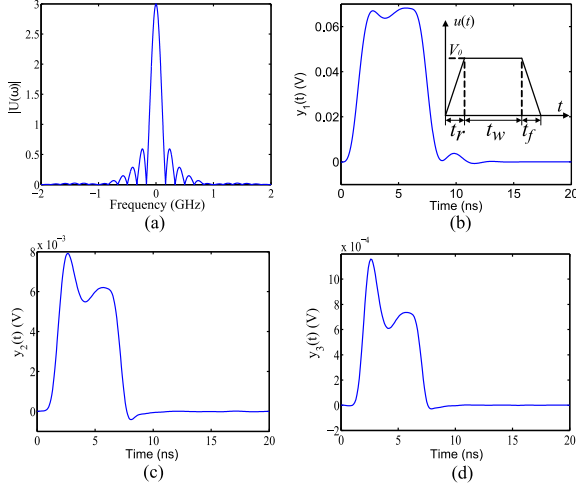

Fig. 7. Input and output signal of the benchmark nonlinear system as shown in Fig. 2. (a) Spectrum of the rectangular pulse input. Time domain output: (b) linear response $y_1(t)$; (c) second-order response $y_2(t)$; (d) third-order response $y_3(t)$. The inset in (b) shows the shape of the rectangular pulse with raise and fall time $t_r = t_f = 1$ ns, and width $t_w = 5$ ns.
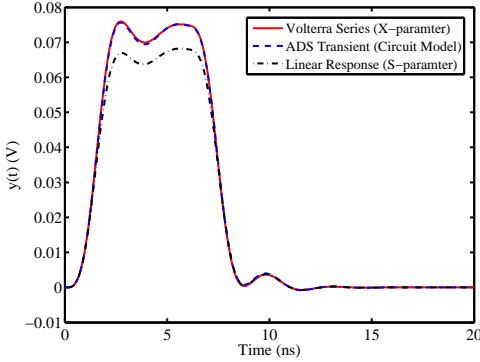

Fig. 8. Comparison of the time domain output of the benchmark nonlinear system as shown in Fig. 2 calculated by the Volterra series representation and ADS transient simulator.

B. Low Noise Amplifier

1) Frequency Domain Volterra Kernel: The second numerical example is a low noise amplifier (LNA). The amplifier schematic used in this work is taken from *X-parameter generation tutorial* of the example directory of ADS [32]. The inset in Fig. 9(a) shows the macro-model of the LNA. The saturation

limit of input is 70 mV. The 3-tone X-parameters are generated with the same frequency sweep scheme shown in Tab. II. The power of each tone is set to $P_{in} = \{-30, -20\}$ dBm. The proposed method is used to extract Volterra kernels from X-parameters. Fig. 9(a) and (b) show the magnitude and phase of the first-order Volterra kernel H_1. They agree well with the small signal S-parameters. This is reasonable since X-parameters becomes S-parameters in the small signal limit. Fig. 9(c) and (d) present the magnitudes of the second-order Volterra kernel and a slice of the third-order Volterra kernel with $\omega_3 = 0.5$ GHz, respectively. Again, H_2 has two symmetry planes due to permutation and conjugate symmetry while H_3 only has one symmetry plane due to the lost of the conjugate symmetry.
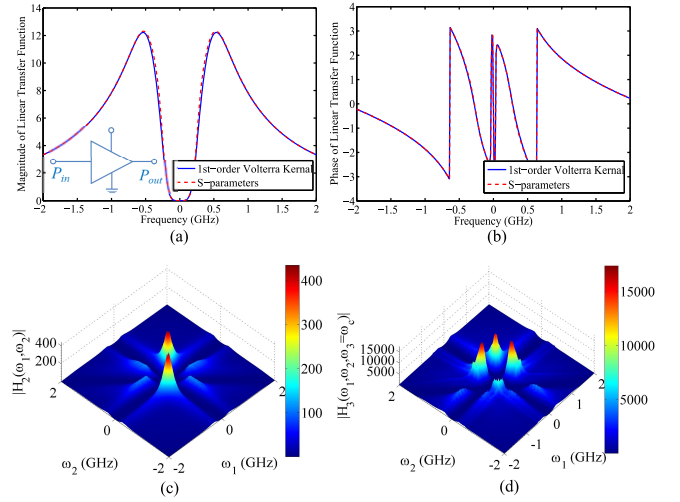

Fig. 9. Volterra kernels of the low noise amplifier (LNA). (a) and (b) are the magnitude and phase of the linear transfer function (first-order Volterra Kernel $H_1(\omega_1)$); (c) magnitude of the second-order Volterra kernel $H_2(\omega_1, \omega_2)$; (d) a slice of the magnitude of the third-order Volterra kernel $H_3(\omega_1, \omega_2, \omega_3 = \omega_c)$ with $\omega_c = 0.5$ GHz. The inset in (a) is the macro-model of the LNA.

2) Time Domain Output: After obtaining the Volterra kernels, different orders of time domain responses are calculated according to (5) and (7). The rectangular pulse shown in the inset of Fig. 7(b) is used with $V_0 = 0.2$ V. Fig. 10 displays the total output $y(t)$ calculated based on the Volterra series representation. It captures the distortion due to nonlinearities and agrees well with the result simulated by the ADS transient simulator with the original circuit model. Fig. 11 shows the time domain output signal calculated based on the Volterra series model with different order and the ADS HB simulator with circuit model. The input signal is a single tone with frequency $f = 1$ GHz. The input power is set to be $P_{in} = -0.5$ dBm so that the LNA works in strong nonlinear region. To fully capture the nonlinear feature of the LNA, higher order Volterra kernels are required. As displayed in Fig. 11, with the increasing of Volterra order, the output signals calculated by the Volterra series model with higher order ($M = 5$ and $M = 7$) agree well with that calculated by ADS HB simulator with circuit model.

3) Computational Cost: Table III shows the computational information for time domain macro-modeling of the LNA by
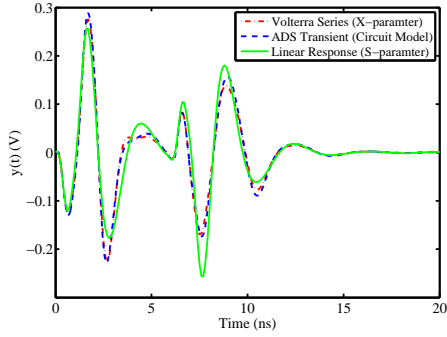
Fig. 10. Comparison of the time domain output of the low noise amplifier calculated by the Volterra series representation and ADS transient simulator.
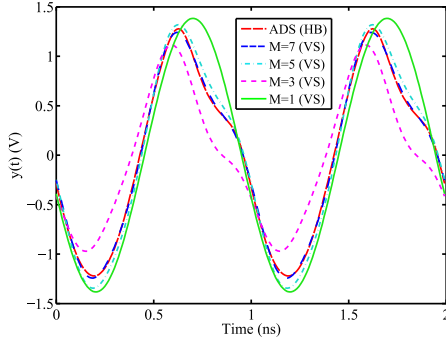

Fig. 11. Time domain output signals calculated based on the Volterra series (VS) model with different order and the ADS harmonic balance (HB) simulator with circuit model. The input signal is a single tone with frequency $f = 1\,\text{GHz}$ and power $P_{in} = -0.5\,\text{dBm}$.

Volterra series model. The computation is implemented in MATALB on a desktop with an Intel i5 3.3 GHz CPU and 16 GB RAM. The most computational consuming parts are the generation of X-parameters and the extraction of Volterra kernels. However, we only need to do these two procedures once. They can be repeatedly used for different types of input. As a blackbox macro-model, the computational cost of Volterra series model does not depend on the original circuit. It only depends on the number of frequency sampling points and the order of Volterra kernels.

TABLE III
COMPUTATIONAL INFORMATION FOR TIME DOMAIN MACRO-MODELING
OF THE LNA BY VOLTERRA SERIES MODEL

Computational Cost	Memory (MB)	CPU Time (min.)
X-parameter Generation	2542.2	273.5
Volterra Kernel Extraction	1907.3	65.7
$y_1(t)$	1.6	0.1
$y_2(t)$	9.6	1.8
$y_3(t)$	143.2	21.6

VI. CONCLUSION

This paper presents a systematic method for extracting Volterra series representation from X-parameters. By completely separating different order of Volterra kernels based on

the least square linear regression method, the complete description of Volterra kernels can be determined very efficiently. Time domain output can be obtained conveniently based on the determined Volterra kernels with arbitrary input. Numerical results show the capability of Volterra series representation for describing nonlinear devices in a broad input power region. The procedure for extracting Volterra kernels with the truncation order $M = 3$ is illustrated in detail. The paper gives the general relationship between Volterra series and X-parameters and the method can be applied to the extraction of higher-order Volterra kernels.

APPENDIX A
OUTPUT FREQUENCIES AND VOLTERRA KERNELS FOR THE THREE-TONE INPUT CASE

For the three-tone input case, the output frequencies are the mixing of the input frequencies $\omega = k_1\omega_1 + k_2\omega_2 + k_3\omega_3$ and can be indexed as $[k_1, k_2, k_3]$. Suppose the maximum mixing order is $M_0 = 3$, the first-order output contains 3 output frequencies and the corresponding 3 Volterra kernels as listed in Tab. IV.

TABLE IV
FREQUENCIES AND VOLTERRA KERNELS INCLUDED IN THE
FIRST-ORDER OUTPUT

Frequency	Notation	Volterra Kernel
ω_1	[1,0,0]	$H_1(\omega_1)$
ω_2	[0,1,0]	$H_1(\omega_2)$
ω_3	[0,0,1]	$H_1(\omega_3)$

The second-order output contains 9 output frequencies and the corresponding 9 Volterra kernels as shown in Tab. V.

TABLE V
FREQUENCIES AND VOLTERRA KERNELS INCLUDED IN THE
SECOND-ORDER OUTPUT

Frequency	Notation	Volterra Kernel
$2\omega_1$	[2,0,0]	$H_2(\omega_1, \omega_1)$
$2\omega_2$	[0,2,0]	$H_2(\omega_2, \omega_2)$
$2\omega_3$	[0,0,2]	$H_2(\omega_3, \omega_3)$
$|\omega_1, \pm\omega_2|$	$[1, \pm1, 0]$	$H_2(\omega_1, \pm\omega_2)$
$|\omega_2, \pm\omega_3|$	$[0, 1, \pm1]$	$H_2(\omega_2, \pm\omega_3)$
$|\omega_1, \pm\omega_3|$	$[1, 0, \pm1]$	$H_2(\omega_1, \pm\omega_3)$

Table VI shows the 22 output frequencies and the corresponding 28 Volterra kernels included in the third-order output.

It should be noticed that both the first-order and the third-order outputs contain the output frequencies ω_1, ω_2, ω_3. Hence, the total number of the output frequencies is 31.

TABLE VI
FREQUENCIES AND VOLTERRA KERNELS INCLUDED IN THE
THIRD-ORDER OUTPUT

Frequency	Notation	Volterra Kernel
ω_1	[1,0,0]	$H_3(\omega_1,\omega_1,-\omega_1),$ $H_3(\omega_1,\omega_2,-\omega_2),$ $H_3(\omega_1,\omega_3,-\omega_3)$
ω_2	[0,1,0]	$H_3(\omega_2,\omega_1,-\omega_1),$ $H_3(\omega_2,\omega_2,-\omega_2),$ $H_3(\omega_2,\omega_3,-\omega_3)$
ω_3	[0,0,1]	$H_3(\omega_3,\omega_1,-\omega_1),$ $H_3(\omega_3,\omega_2,-\omega_2),$ $H_3(\omega_3,\omega_3,-\omega_3)$
$3\omega_1$	[3,0,0]	$H_3(\omega_1,\omega_1,\omega_1)$
$3\omega_2$	[0,3,0]	$H_3(\omega_2,\omega_2,\omega_2)$
$3\omega_3$	[0,0,3]	$H_3(\omega_3,\omega_3,\omega_3)$
$|\omega_1,\pm2\omega_2|$	$[1,\pm2,0]$	$H_3(\omega_1,\omega_2,\omega_2),$ $H_3(\omega_1,-\omega_2,-\omega_2)$
$|2\omega_1,\pm\omega_2|$	$[2,\pm1,0]$	$H_3(\omega_1,\omega_1,\omega_2),$ $H_3(\omega_1,\omega_1,-\omega_2)$
$|\omega_2,\pm2\omega_3|$	$[0,1,\pm2]$	$H_3(\omega_2,\omega_3,\omega_3),$ $H_3(\omega_2,-\omega_3,-\omega_3)$
$|2\omega_2,\pm\omega_3|$	$[0,2,\pm1]$	$H_3(\omega_2,\omega_2,\omega_3),$ $H_3(\omega_2,\omega_2,-\omega_3)$
$|\omega_1,\pm2\omega_3|$	$[1,0,\pm2]$	$H_3(\omega_1,\omega_3,\omega_3),$ $H_3(\omega_1,-\omega_3,-\omega_3)$
$|2\omega_1,\pm\omega_3|$	$[2,0,\pm1]$	$H_3(\omega_1,\omega_1,\omega_3),$ $H_3(\omega_1,\omega_1,-\omega_3)$
$|\omega_1,\pm\omega_2\pm\omega_3|$	$[1,\pm1,\pm1]$	$H_3(\omega_1,\omega_2,\omega_3),$ $H_3(\omega_1,\omega_2,-\omega_3),$ $H_3(\omega_1,-\omega_2,\omega_3),$ $H_3(\omega_1,-\omega_2,-\omega_3)$

especially, we thank David Root, Loren Betts, Steve Fulwider and Bill Wallace of Keysight for fruitful discussions, insightful comments and helpful suggestions. X-parameters is a registered trademark of Agilent Technologies.segment>

REFERENCES

[1] S. Tan and L. He, *Advanced Model Order Reduction Techniques in VLSI Design*, Cambridge, U.K.: Cambridge Univ. Press, 2007.

[2] M. A. Farhan, E. Gad, M. S. Nakhla, and R. Achar, "Fast simulation of microwave circuits with nonlinear terminations using high-order stable methods," *IEEE Trans. Microw. Theory Techn.*, vol. 61, no. 1, pp. 360–371, Jan. 2013.

[3] D. Spina, D. De Jonghe, D. Deschrijver, G. Gielen, L. Knockaert, and T. Dhaene, "Stochastic macromodeling of nonlinear systems via polynomial chaos expansion and transfer function trajectories," *IEEE Trans. Microw. Theory Techn.*, vol. 62, no. 7, pp. 1454–1460, Jul. 2014.

[4] Y. Fang, M. C. E. Yagoub, F. Wang, and Q. J. Zhang, "A new macromodeling approach for nonlinear microwave circuits based on recurrent neural networks," *IEEE Trans. Microw. Theory Techn.*, vol. 48, no. 12, pp. 2335–2344, Dec. 2000.

[5] M. Ma and R. Khazaka, "Sparse macromodeling for parametric nonlinear networks," *IEEE Trans. Microw. Theory Techn.*, vol. 54, no. 12, pp. 4305–4315, Dec. 2006.

[6] P. Li and L. Pileggi, "Compact reduced-order modeling of weakly nonlinear analog and RF circuits," *IEEE Trans. Comput.-Aided Design Integr. Circuits Syst.*, vol. 24, no. 2, pp. 184–203, Feb. 2005.

[7] J. R. Phillips, "Projection-based approaches for model reduction of weakly nonlinear, time-varying systems," *IEEE Trans. Comput.-Aided Design Integr. Circuits Syst.*, vol. 22, no. 2, pp. 171–187, Feb. 2003.

[8] T. Palenius and J. Roos, "Comparison of reduced-order interconnect macromodels for time-domain simulation," *IEEE Trans. Microw. Theory Techn.*, vol. 52, no. 9, pp. 2240–2250, Sep. 2004.

[9] A. Astolfi, "Model reduction by moment matching for linear and nonlinear systems," *IEEE Trans. Autom. Control*, vol. 55, no. 10, pp. 2321–2336, Oct. 2010.

[10] F. Ferranti, M. Nakhla, G. Antonini, T. Dhaene, L. Knockaert, A. E. Ruehli, "Interpolation-based parameterized model order reduction of delayed systems," *IEEE Trans. Microw. Theory Techn.*, vol. 60, no. 3, pp. 431–440, Feb. 2012.

[11] M. Rewienski and J. White, "A trajectory piecewise-linear approach to model order reduction and fast simulation of nonlinear circuits and micromachined devices," *IEEE Trans. Comput.-Aided Design Integr. Circuits Syst.*, vol. 22, no. 2, pp. 155–170, Feb. 2003.

[12] Q. I. Dai, Y. H. Lo, W. C. Chew, Y.G. Liu, and L. J. Jiang, "Generalized modal expansion and reduced modal representation of 3-D electromagnetic fields", *IEEE Trans. Antennas Propag.*, vol. 58, pp. 3856–3864, Feb. 2014.

[13] J. Schutt-Aine, T. Jilin, C. Kumar, and F. Al-Hawari, "Blackbox macromodel with S-parameters and fast convolution," in *Proc. 12th IEEE Workshop Signal Propag. Interconnects*, pp. 1–4, May 2008.

[14] B. Gustavsen and A. Semlyen, "Fast passivity assessment for S-parameter rational models via a half-size test matrix," *IEEE Trans. Microw. Theory Techn.*, vol. 56, no. 12, pp. 2701–2708, Dec. 2008.

[15] D. Deschrijver, K. Crombecq, H. M. Nguyen and T. Dhaene, "Adaptive sampling algorithm for macromodeling of parameterized S-parameter responses," *IEEE Trans. Microw. Theory Techn.*, vol. 59, no. 1, pp. 39–45, Nov. 2010.

[16] T. Dhaene, D. Deschrijver and N. Stevens, "Efficient algorithm for passivity enforcement of S-parameter-based macromodels" *IEEE Trans. Microw. Theory Techn.*, vol. 57, no. 2, pp. 415–420, Jan. 2009.

[17] D. E. Root, J. Verspecht, D. Sharrit and J. Wood, "Broad-band polyharmonic distortion behavioral models from fast automated simulations and large signal vectorial network measurements," *IEEE Trans. Microw. Theory Tech.* pp. 3656–3664, 2005.

[18] J. E. Schutt-Aine, P. Milosevic and W. T. Beyene, "Modeling and simulation of high speed I/O links using X parameters," in *IEEE Conf. on Electrical Performance of Electronic Packaging and Systems (EPEPS)*, pp. 29–32, 2010.

[19] J. Verspecht, J. Horn, L. Betts, D. Gunyan, R. Pollard, C. Gillease and D. E. Root, "Extension of X-parameters to include long-term dynamic memory effects," *IEEE MTT-S Int. Microw. Symp. Dig.*, pp. 601–604, Jun. 2009.

[20] J. Verspecht, J. Horn and D. E. Root, "A simplified extension of X-parameters to describe memory effects for wideband modulated signals," in *Proc. 75th ARFTG Conf. Dig.*, pp. 1–6, May. 2010.

[21] J. Verspecht, D. E. Root and T. Nielsen, "Dynamic X-parameters: Behavioral modeling in the presence of long term memory effects," *The 7th German Microwave Conference (GeMiC)*, pp. 1–4, 2012.

[22] A. Zhu and T. J. Brazil, "Behavioral modeling of RF power amplifiers based on pruned volterra series," *IEEE Microw. Wireless Compon. Lett.*, vol. 14, no. 12, pp. 563–565, Dec. 2004.

[23] H. Liu, and N. Wong, "Autonomous Volterra algorithm for steady-state analysis of nonlinear circuits," *IEEE Trans. Comput.-Aided Design Integr. Circuits Syst.*, vol. 32, no. 6, pp. 858–868, Jun. 2013.

[24] J. A. Cherry, "Distortion Analysis of Weakly Nonlinear Filters Using Volterra Series," Master Thesis, Carleton University, Canada, 1994.

[25] X. Y. Z. Xong, L. J. Jiang, J. Shutt-Aine, and W. C. Chew, "Blackbox macro-modeling of the nonlinearity based on Volterra series representation of X-parameters," in *IEEE Conf. Electrical Performance of Electronic Packaging and Systems (EPEPS)*, pp. 85–88, Oct. 2014.

[26] R. H. Flake, "Volterra series representation of nonlinear systems," *IEEE Trans. Appl. Ind.*, vol. 81, pp. 330–335, Jan. 1963.

[27] Verspecht and D. Root, "Polyharmonic distortion modeling," *IEEE Microw. Mag.*, vol. 7, no. 3, pp. 44–57, Jun. 2006.

[28] D. E. Root, J. Verspecht, J. Horn and M. Marcu, *X-Parameters: Characterization, Modeling, and Design of Nonlinear RF and Microwave Components* Cambridge University Press, Sep, 2013.

[29] M. Schetzen, *The Volterra and Wiener Theories of Nonlinear Systems*, Krieger Publishing Company, 2006.

[30] W. J. Rugh, *Nonlinear System Theory: The Volterra/Wiener Approach*, The Johns Hopkins University Press, 1981.

[31] S. Boyd, Y. S. Tang and L. O. Chua, "Measuring Volterra kernels", *IEEE Trans. Circuits and Systems*, CAS-30, pp.571–577, 1983.

[32] *Agilent Advanced Design System*, Version 2011.10. Copyright (c) 1983–2011, Agilent Technologies.

[33] N. Huang and L.J. Jiang, "Simulations of pulse signals with X-parameters," in *IEEE Conf. on Electrical Performance of Electronic Packaging and Systems (EPEPS)*, pp. 23–26, 2011.

Xiaoyan Y. Z. Xiong (S'12-M'15) received the B.S. degree from Southwest Jiaotong University, Chengdu, China, in 2008, the M.S. degree from Peking University, Beijing, China, in 2011, and Ph.D degree from the University of Hong Kong, Hong Kong, in 2015. She has been with the Center of Electromagnetics and Optics, University of Hong Kong, and the Center for Computational Electromagnetics and Electromagnetics Laboratory, University of Illinois at Urbana-Champaign, since 2011 and 2014, respectively. She is currently a postdoctoral fellow at the University of Hong Kong, Hong Kong.

In 2016, she received the Young Scientist Award in the International Symposium on Electromagnetic Theory (EMTS), Espoo, Finland. In 2014, she received the Best Oral Paper Award in the IEEE Conference on Electrical Performance of Electronic Packaging and Systems (EPEPS), Portland, Oregon, USA. In the 30th International Review of Progress in Applied Computational Electromagnetics (ACES), Jacksonville, Florida, USA, 2014, she won the Best Student Paper Award. She is also the Champion of Student Paper Competition of the AP Section of the IEEE HK AP/MTT Postgraduate Conference, Hong Kong, 2013. Her research interests include high-power microwave devices, computational electromagnetics, metamaterials, nonlinear optics and nonlinear circuits.

José E. Schutt-Ainé (S'86-M'86-SM'98-F'07) received the B.S. degree in electrical engineering from the Massachusetts Institute of Technology, Cambridge, in 1981, and the M.S. and Ph.D. degrees from the University of Illinois at Urbana-Champaign (UIUC), Urbana, in 1984 and 1988, respectively. He joined the Hewlett-Packard Technology Center, Santa Rosa, CA, as an Application Engineer, where he was involved in research on microwave transistors and high-frequency circuits. In 1983, he joined UIUC, and then joined the Electrical and Computer Engineering Department as a member of the Electromagnetics and Coordinated Science Laboratories, Urbana, where he is currently involved in research on signal integrity for high-speed digital and high-frequency applications. He is a consultant for several corporations. His current research interests include the study of signal integrity and the generation of computer-aided design tools for high-speed digital systems. Dr. Schutt-Ain was a recipient of several research awards, including the 1991 National Science Foundation (NSF) MRI Award, the National Aeronautics and Space Administration Faculty Award for Research in 1992, the NSF MCAA Award in 1996, and the UIUC-National Center for Superconducting Applications Faculty Fellow Award in 2000.

Li Jun Jiang (S'01-M'04-SM'13) received the B.S. degree in electrical engineering from the Beijing University of Aeronautics and Astronautics in 1993, the M.S. degree from the Tsinghua University in 1996, and Ph.D from the University of Illinois at Urbana-Champaign in 2004. From 1996 to 1999, he was an application engineer with the Hewlett-Packard Company. Since 2004, he has been the postdoctoral researcher, the research staff member, and the senior engineer at IBM T.J. Watson Research Center. Since the end of 2009, he is an Associate Professor with the Department of Electrical and Electronic Engineering at the University of Hong Kong. From Sept. 2014 to Mar. 2015, he is also a visiting scholar at the University of California at Los Angeles.

In 1998 he received the HP STAR Award. In 2003 he received the IEEE MTT Graduate Fellowship Award, and in 2004 the Y.T. Lo Outstanding Research Award. In 2008 he received the IBM Research Technical Achievement Award. He is the IEEE Senior Member, the Associate Editor of IEEE Transactions on Antennas and Propagation, the Editor of Progress in Electromagnetics Research, the Associate Guest Editor of the Proceedings of IEEE Special Issue in 2011-2012, an IEEE AP-S Member, an IEEE MTT-S member, an ACES member, and a member of Chinese Computational Electromagnetics Society. He was the Semiconductor Research Cooperation (SRC) Industrial Liaison for several academic projects. He was the TPC member of IEEE Electrical Design for Advanced Packaging and Systems (EDAPS) since 2010, the TPC member of 2013 IEEE International Conference on Microwave Technology & Computational Electromagnetics (ICMTCE), the scientific committee member of 2010 Workshop on Simulation and Modeling of Emerging Electronics (SMEE), the special session organizers of IEEE EDAPS, the International Review of Progress in Applied Computational Electromagnetics (ACES), Asia-Pacific Radio Science Conference (AP-RASC), the co-organizer of HKU Computational Science and Engineering Workshops in 2010-2012, the TC-9 and TC-10 member of IEEE EMC-S since 2011, the TPC Chair of the 7th International Conference on Nanophotonics (ICNP), the TPC member of the 3rd Conference on Advances in Optoelectronics and Micro/Nano Optics (AOM), the Co-chair of International Workshop on Pulsed Electromagnetic Field at the Delft, the Netherlands, 2013, the Chair of 14th IEEE Hong Kong AP/MTT Postgraduate Conference, and session chairs of many international conferences. He also serves as the reviewer of IEEE Transactions on several topics, and other primary electromagnetics and microwave related journals.

His research interests focus on electromagnetics, computational electromagnetics, IC signal/power integrity, IC EMC/EMI, antennas, multi-physics modeling, etc.

Weng Cho Chew (S'79-M'80-SM'86-F'93) received the B.S.E.E., M.S.E.E. and Engineer's degrees and Ph.D.E.E. degree in 1976, 1978, and 1980, respectively, from MIT. He joined the U of Illinois in 1985.

He served as the Dean of Engineering at Hong Kong U (2007-2011). Before 1985, he was a department manager and a program leader at Schlumberger-Doll Research (1981-1985). He served on the IEEE Adcom for AP Society as well as GRS Society. He is active with various journals, societies, and international collaboration.

His research interests are in wave physics and mathematics of inhomogeneous media for sensing applications, IC, and antenna applications, as well as fast algorithms for scattering and radiation problems. He originated several fast algorithms for electromagnetics scattering and inverse problems. His research group solved dense matrices with tens of millions of unknowns first ever for scattering problems. His recent interest is in multi-physics phenomena in nano-eletronics and N/MEMS.

He authored and co-authored books entitled Waves and Fields in Inhomogeneous Media, Fast and Efficient Methods in Computational Electromagnetics, and Integral Equation Methods for Electromagnetic and Elastic Waves, and over 400 journal publications, 450 conference publications and ten book chapters.

He is a Fellow of IEEE, OSA, IOP, EMA, HKIE, and was an NSF Presidential Young Investigator (USA). He received the Schelkunoff Best Paper Award for AP Transaction, IEEE Graduate Teaching Award, UIUC Campus Wide Teaching Award, and IBM Faculty Awards. He was a Founder Professor of the College of Engineering (2000-2005), and the First Y.T. Lo Chair Professor (2005-2009), and an IEEE Distinguished Lecturer (2005-2007), Cheng Tsang Man Visiting Professor at NTU in Singapore (2006). In 2002, ISI Citation elected him to be among the Most Highly Cited Authors. He received the AP-Society Chen-To Tai Distinguished Educator Award (2008), and was on the BoD of Applied Science Technology Research Institute, Hong Kong. He is currently the Editor-in-Chief of PIER journals, and the Chair of the IEEE Joint Chapter on AP Society, GRS Society, and Photonic Society, which hosts a seminar series. Recently, he has been elected to the US National Academy of Engineering. He is a Fisher Distinguished Professor of Engineering at UIUC.